ASEG-PESA 2013
'THE EUREKA MOMENT'
11-14 AUGUST 2013 • MELBOURNE, AUSTRALIA

3D inversion of ZTEM data for uranium exploration

Yutaka Sasaki
Kyushu University
Motooka,, Nishi-ku, Fukuoka
819-0395, Japan
sasaki@mine.kyushu-u.ac.jp

Myeong-Jong Yi
Korea Institute of Geoscience & Mineral Resources
Gwahang-no, Yuseong-gu, Daejeon 305-350, Korea
muse@kigam.re.kr

Jihyang Choi
Korea Institute of Geoscience & Mineral Resources
Gwahang-no, Yuseong-gu, Daejeon 305-350, Korea
cecile137@gmail.com

SUMMARY

We present a Gauss-Newton-based 3D inversion method for airborne ZTEM (Z-axis Tipper Electromagnetic) data to define resistivity structure relating to uranium deposits in the Athabasca Basin of Saskatchewan, Canada. The geophysical targets in this region can be represented by conductive plunging dykes in a resistive basement beneath a thick, more resistive overburden. We demonstrate using synthetic examples the effectiveness of the inversion method for detecting and delineating the target dykes and discuss how the inversion results are affected by various factors. It is shown that the dykes can be well imaged to depths more than 2 km even for the data from 200-m receiver height, provided the flight line is oriented perpendicular to the strike, and that the inversion results are relatively robust to the choice of the starting model. It is also shown that topographic effects are not serious for detecting the dykes at depth, because topographic effects are more significant at higher frequencies, while the sensitivity to the dykes increases with decreasing frequencies. One important finding is that if the flight line is oblique to the strike, the dependence of the starting model increases and the overall resolution decreases, compared to the 2D case, due to 3D effects.

Key words: ZTEM, tipper, 3D inversion, uranium exploration.

INTRODUCTION

ZTEM (Z-axis Tipper Electromagnetic) system has been used for mineral exploration since 2007 (Lo and Zang, 2008). The main advantage, compared to controlled-source airborne EM systems, is a greater depth of investigation which is the consequence of utilizing natural plane-wave excitation. The vertical component of the magnetic field is recorded using an air-core coil towed behind a helicopter, while the two orthogonal horizontal fields are recorded at a fixed base station on the ground. ZTEM data are commonly interpreted using a 2D inversion method that was modified from the one used for magnetotelluric (MT) data (Legault *et al*., 2009). Holtham and Oldenburg (2010) attempted a joint inversion of ZTEM and MT data, showing that the combination of sparse MT data with economical spatial acquisition of ZTEM data creates a cost-effective exploration technique. Kaminski *et al*. (2012) examined the effect of topography on inversion results.

The purpose of this study is to develop an interpretation technique for ZTEM data to explore for uranium deposits in the Athabasca Basin of Saskatchewan, Canada. Uranium deposits within this region are associated with the unconformity between Proterozoic sandstones and the underlying Archean-Paleoproterozoic basement rocks, and they occur along basement faults and fracture zones (Legault *et al*., 2009). Thus, the targets for EM surveys are represented by conductive plunging dykes in a basement beneath a thick resistive overburden. In this paper, we introduce a 3D inversion algorithm that uses a Gauss-Newton approach and calculates full Jacobians, and examine the effectiveness and limitations of the method in resolving target dykes associated with unconformity-type uranium deposits.

ZTEM RESPONSE

For the plane-wave fields that propagate downward into the earth, the magnetic-field components, H_x, H_y, and H_z, are linearly related as

$$H_z = T_{zx}H_x + T_{zy}H_y, . \quad (1)$$

where T_{zx} and T_{zy} are the components of a complex transfer function, which are called the tipper (Vozoff, 1972). To solve for T_{zx} and T_{zy}, we need two different source polarizations. Using the superscripts 1 and 2 to designate fields generated by two polarizations, we have the tipper components

$$T_{zx} = (H_y^2 H_z^1 - H_y^1 H_z^2)/D , \quad (2)$$

$$T_{zy} = (H_x^1 H_z^2 - H_x^2 H_z^1)/D , \quad (3)$$

where

$$D = H_x^1 H_y^2 - H_x^2 H_y^1 . \quad (4)$$

The tipper depends on the coordinate directions but is independent of the source polarization. One unique feature of the tipper is that the presence of lateral resistivity variations gives rise to an anomalous response (or vertical field), while 1D layered structures produce no response (Labson *et al*., 1985). The forward modelling of the tipper is based upon a 3D MT modelling algorithm that employs a staggered-grid finite-difference method (Sasaki, 2001). We modified it so that the vertical magnetic fields in the air can be computed.

INVERSION METHOD

Our inversion algorithm is based upon a Gauss-Newton approach where a model **m** is sought such that it adequately reproduces the data **d**. The data consist of the real (in-phase) and imaginary (quadrature) parts of T_{zx} and T_{zy} for given frequencies. The inverse problem is formulated as an optimization problem in which the objective functional to be minimized is defined as

$$\phi(\mathbf{m}) = \left\| \mathbf{W}\left[\mathbf{d} - \mathbf{f}(\mathbf{m})\right] \right\|^2 + \alpha^2 \left\| \mathbf{Cm} \right\|^2 + \alpha^2 c^2 \left\| \mathbf{m} - \mathbf{m}_b \right\|^2 . \quad (5)$$

In the above, **f**(**m**) represents the ZTEM responses obtained from 3D forward modelling, **C** is a spatial second-order finite-difference operator to quantify the model roughness, and $\mathbf{m}_b$ is a reference model (or a priori information). α is a regularization parameter that trades off between the data misfit and model constraint, and c is an adjustable constant that assigns a relative weight on the closeness to the reference model. The matrix **W** is diagonal and represents the data weights assigned according to the estimated uncertainty for each datum.

The function **f**(**m**) is linearized with respect to the initial model $\mathbf{m}^{(0)}$, and the perturbation $\Delta\mathbf{m}$ is sought such that the linearized objective functional is minimized. At the k-th iteration, the minimization of the objective functional is equivalent to obtaining the least-squares solution of a rectangular (over-determined) system of equations

$$\begin{bmatrix} \mathbf{WA} \\ \alpha\,\mathbf{C} \\ \alpha\, c\,\mathbf{I} \end{bmatrix} \{\Delta\mathbf{m}\} = \begin{Bmatrix} \mathbf{W}\Delta\mathbf{d} \\ -\alpha\,\mathbf{C}\mathbf{m}^{(k)} \\ \alpha\, c(\mathbf{m}^{(0)} - \mathbf{m}^{(k)}) \end{Bmatrix}, \qquad (6)$$

where $\Delta\mathbf{d}$ is the difference between the observed and predicted data, **A** is the Jacobian of the ZTEM responses with respect to the logarithm of the resistivity, and **I** is the identity matrix. Note that the initial model is used as the reference model in equation (6). The Jacobian can be obtained by making additional forward calculation for a (fictitious) vertical magnetic dipole placed at each receiver location, based on the reciprocity relation (McGillivray *et al.*, 1994). We solve equation (6) using the modified Gram–Schmidt method.

SYNTHETIC EXAMPLES

We test our inversion algorithm on 2D and 3D models relating to unconformity-type uranium deposits and examine how inversion results are affected by the starting model, receiver height, topography, and the orientation of the flight line with respect to the strike. For the forward modelling, the earth is discretized with a grid of 81 x 81 x 45 (295,245) cells.

Multiple dykes with irregular overburden

As shown in Figure 1, our first model has four 10-ohm-m dykes in a 2000-ohm-m host medium beneath a 5000-ohm-m overburden with variable thickness. The thickness of dykes is 50 m, and their depth extent is 2.5 km. It is assumed that the strike is in the y direction, and the flight is in the x direction. The sampling spacing is 100 m. We consider five frequencies: 30, 45, 90, 180, and 360 Hz. Figure 2 shows the in-phase and quadrature components of T_{zx} at 50 m receiver height above the ground. Note that these responses are solely due to induced currents in the y direction. One unique feature of the tipper for such 2D dyke models is that its magnitude increases with decreasing the frequency.

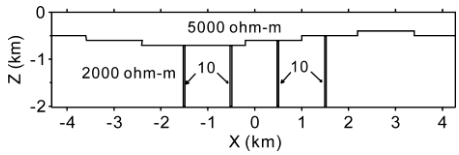

Figure 1. 2D model with four dykes. The thickness of dykes is 50 m. The vertical extent of dykes is 2.5 km.

In the inversion, the model region is divided into 2070 (46 x 5 x 9) blocks, with a minimum size of 200 x 2400 x 200 m. All the boundaries of blocks do not coincide with those of the true model. The number of real-valued data points is 1620, including T_{zy} components which are null for 2D structures. The regularization parameter α was set to values of 0.02, 0.01, for the first two iterations, and 0.005 for the remaining iterations. The constant c was fixed at 0.5 throughout this study. Figure 3 shows a comparison of the inversion results obtained from the data sets at four different receiver heights: 50, 80, 110, 200 m. The starting model is a 3000-ohm-m half-space covered by a 4000-ohm-m overburden with thickness of 600 m. It is seen from Figure 3 that the outside dykes are well imaged to depths more than 2 km, but the resolution of the inside dykes decreases gradually with increasing the receiver height. For all cases, the RMS data misfit converges to a value between 0.010 and 0.011 after four to six iterations, which is almost identical to the given noise level 0.01.

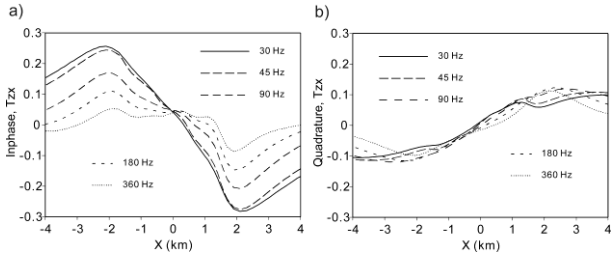

Figure 2. Inphase (a) and quadrature (b) component profiles of ZTEM responses at frequencies of 30, 45, 90, 180, and 360 Hz. The receiver height is 50 m.

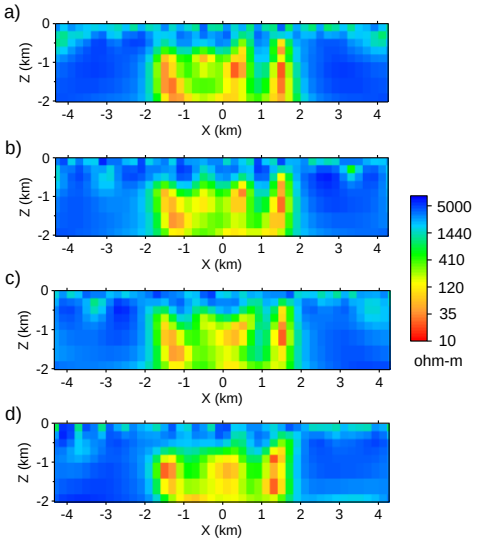

Figure 3. Resistivity images obtained from inversion of ZTEM data at receiver heights of (a) 50 m, (b) 80 m, (c) 110 m, and (d) 200 m. The starting model is a 3000-ohm-m half-space beneath a 4000-ohm-m overburden with thickness of 600 m.

Effect of topography

The model shown in Figure 4 has a trapezoidal hill with a top width of 200 m, a bottom width of 4.2 km, and 300 m height. There are two 10-ohm-m dykes in a 1000-ohm-m host medium. The receiver clearance is 100 m. Figure 5 shows

the resistivity images obtained from two inversions that assume the flat surface and account for topography. The starting models have 2000 ohm-m resistivity. One can see that although high-resistivity artefacts appear near the foot of the hill when assuming a flat surface, there is no significant difference in resolving dykes at depth whether or not topography is accounted for. This is because the topographic effect is more significant at higher frequencies, while the tippers have a higher sensitivity to dykes at lower frequencies as shown before.

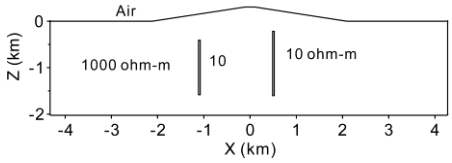

Figure 4. 2D topographic model with two dykes.

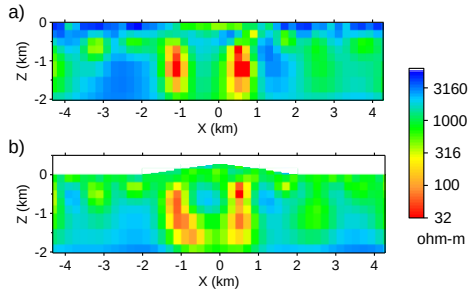

Figure 5. Inversion results obtained, (a) assuming a flat surface and (b) accounting for topography. The starting model has a constant resistivity of 2000 ohm-m.

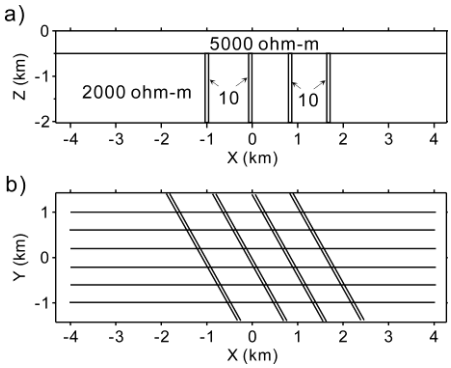

Figure 6. Cross section (a) and plan view (b) of a multiple dyke model. The flight line spacing is 400 m, and the receiver height is 100 m.

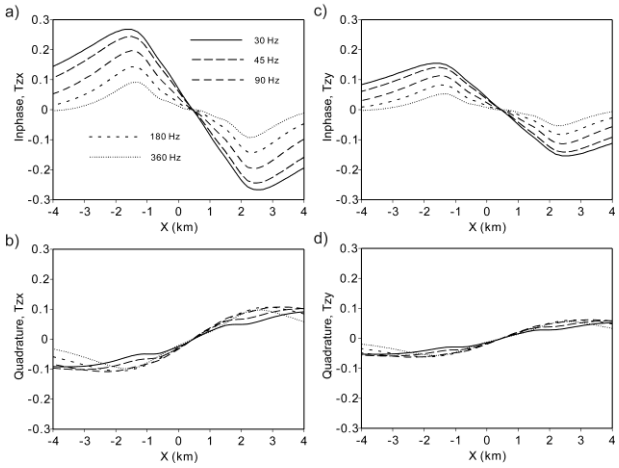

Figure 7. Inphase (a, c) and quadrature (b, d) component profiles of ZTEM responses at y = -200 m and frequencies of 30, 45, 90, 180, and 360 Hz. The left column corresponds to *Tzx*, the right column *Tzy*,

3D survey over multiple dykes

The next example involves multiple dykes again, but their strike is 60 degrees from the flight direction. The cross section and plan view of the model is shown in Figure 6. Four 10-ohm-m dykes are embedded in a 2000-ohm-m host medium beneath a 5000-ohm-m overburden with thickness 500 m. The dykes are 50 m thick. The survey consists of six 8-km long flight lines in the *x* direction, with 100 m sampling spacing and 400 m line spacing. The receiver height is 100 m. Figure 7 shows the T_{zx} and T_{zy} profiles at *y* = -200 m and frequencies of 30, 45, 90, 180, and 360 Hz. It is important to note that the T_{zx} profiles are similar to the 2D responses shown in Figure 2, but that the T_{zy} responses are also significant, mainly due to galvanic effects.

In the inversion, the earth was discretized into 7360 (46 x 16 x 10) blocks, with the smallest blocks of 200 m on a side. The total number of real-valued data is 9720. The inversions were performed using three starting models: (1) 2000-ohm-m half-space beneath 5000-ohm-m overburden with thickness 600 m, (2) 3000-ohm-m half-space beneath 4000-ohm-m overburden with thickness 600 m, and (3) 3500-ohm-m half-space. Figure 8 shows the cross sections (along *y* = -100 m and -900 m) and plan view map (at 700 m depth) of the model obtained using the first starting model. Note that this starting model is identical to the true background structure except for the overburden thickness. It can be seen that the clear indications corresponding to the outside dykes are limited to depths of about 1 km, while a low-resistivity zone at depth is concentrated in between the inside dykes. It is evident that the depth resolution is lower than that for the 2D case (Figure 3) in which the anomalous responses are solely due to induction effects. Figures 9 and 10 show the inversion results from the starting models (2) and (3), respectively. One can see that the overall resolution decreases further, implying that choosing the starting model is important for complicated 3D structures.

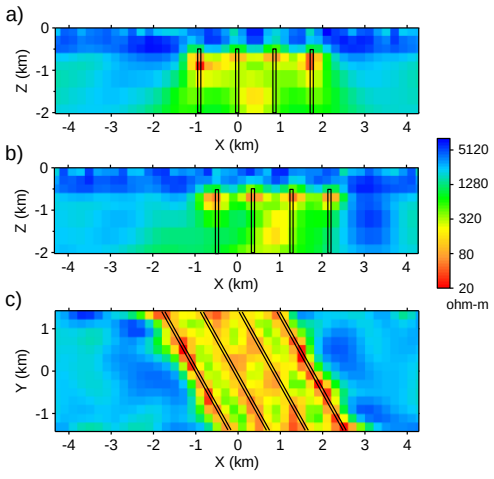

Figure 8. Cross sections (a, b) and plan view map (c) of the recovered resistivity. Cross sections (a) and (b) are along *y* = -100 m and *y* = -900 m, respectively. Plan view

is at a depth of 700 m. The starting model is a 2000-ohm-m half-space beneath a 5000-ohm-m overburden with thickness of 600 m. The black lines indicate the locations of the dykes.

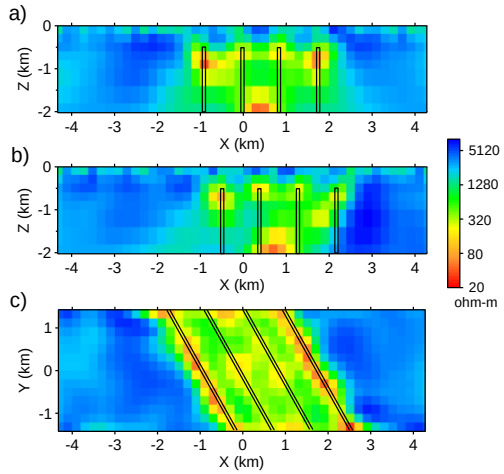

Figure 9. Same as in Figure 8, but the starting model is a 3000-ohm-m half-space beneath a 4000-ohm-m overburden with thickness of 600 m..

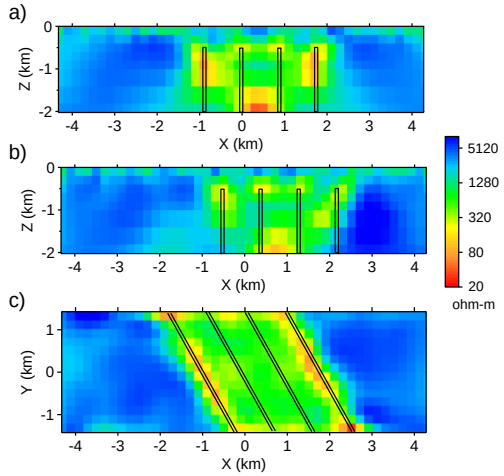

Figure 10. Same as in Figure 8, but the starting model is a 3500-ohm-m half-space.

CONCLUSIONS

We have developed an inversion method to recover 3D distributions of the resistivity from ZTEM data. The method uses a Gauss-Newton approach in which full Jacobians are calculated by taking advantage of the reciprocity relation between the source and receiver. Synthetic examples show that if the survey line is perpendicular to the strike, conductive dykes covered by a thick overburden can be well defined to depths more than 2 km even if the starting model is not close to the true background structure. However, if the dykes are oblique to the survey lines, the resolution to dykes decreases, depending upon the starting model, due to 3D effects. One remedy for this weakness is to collect audio-frequency MT data together with ZTEM data and to carry out a joint inversion of both data sets.

ACKNOWLEDGMENTS

One of the authors (Y.S.) would like to thank Akihiko Chiba of Sumiko Resources Exploration & Development Co., Ltd. for his support.

REFERENCES

Holtham, E. and Oldenburg, D.W., 2010, Three-dimensional inversion of MT and ZTEM data: 80th Meeting, SEG, Denver, Expanded Abstracts, 655-659.

Kaminski, V., Sattel, D., and Witherly, K., 2012, The effect of topography on ZTEM inversions: 74th Conference, EAGE, Copenhagen, Extended Abstracts, A016.

Labson, V.F., Becker, A., Morrison, H.F., and Conti, U., 1985, Geophysical exploration with audio-frequency natural magnetic fields: Geophysics, 50, 656-664.

Legault, J.M., Kumar, H., Milicevic, B., and Wannamaker, P., 2009, ZTEM tipper AFMAG and 2D inversion results over an unconformity uranium target in northern Saskatchewan: 79th Meeting, SEG, Houston, Expanded Abstracts, 1277-1281.

Lo, B. and Zang, M., 2008, Numerical modeling of Z-TEM (airborne AFMAG) response to guide exploration strategies: 78th Meeting, SEG, Las Vegas, Expanded Abstracts, 1098-1102.

McGillivray, P.R., Oldenburg, D.W., Ellis, R.G., and Habashy, T.M., 1994, Calculation of sensitivities for the frequency-domain electromagnetic problem: Geophysical Journal International, 116, 1-4.

Sasaki, Y., 2001, Full 3-D inversion of electromagnetic data on PC: Journal of Applied Geophysics, 46, 45-54.

Vozoff, K., 1972, The magnetotelluric method in the exploration of sedimentary basins: Geophysics, 37, 98-141.